*Desalination and Water Treatment*
www.deswater.com
doi: 10.5004/dwt.2021.26507

209 (2021) 155–169
January

# A new synthesis of $Fe_{1-x}$–$Mn_xO_3$/PVA nanocomposites for the removal of heavy metals from water

Zahid Wahab[a], Mohsan Nawaz[a,*], M.I. Khan[b], Ali Bahader[a], Abdul Niaz[c], Abdur Rahim[d,*], Muhammad Ismail[b], Ata Ur Rehman[b], Rongchao Jin[e]

[a]*Department of Chemistry, Hazara University Mansehra, Khyber Pakhtunkhwa, Pakistan, emails: mohsannawaz@hotmail.com (M. Nawaz), zahidwahabmarwat@gmail.com (Z. Wahab), alibahader@gmail.com (A. Bahader)*
[b]*Department of Chemistry, Kohat University of science and Technology, Kohat – 26000, Khyber Pakhtunkhwa, Pakistan, emails: gorikhan@hotmail.com (M.I. Khan), ismailkust@yahoo.com (M. Ismail), ataur.rehman99@yahoo.com (A.U. Rehman)*
[c]*Department of Chemistry, UST, Bannu, Pakistan, email: niazchemist@hotmail.com (A. Niaz)*
[d]*Interdisciplinary Research Center in Biomedical Materials, COMSATS University Islamabad, Lahore, Pakistan, email: rahimkhan533@gmail.com (A. Rahim)*
[e]*Department of Chemistry, Carnegie Mellon University, Pittsburgh, PA 15213, United States of America, email: rongchao@andrew.cmu.edu (R. Jin)*

Received 28 November 2019; Accepted 24 August 2020

**ABSTRACT**

In the present work, an eco-friendly method is used for the synthesis of $Fe_{1-x}$–$Mn_xO_3$ nanoparticles and $Fe_{1-x}$–$Mn_xO_3$/PVA nanocomposites, where x represents the different concentration of *Zanthoxylum armatum* extract as a stabilizer. Formation of the respective nanomaterials and their nano-composites were confirmed by UV-visible spectroscopy while surface functionality ere confirmed by Fourier transform infrared spectroscopy. Transmission electron microscopy and X-ray diffraction were used to reveal the surface morphology and crystallinity of the particles. The synthesized materials were then used as adsorbents for removal of Pb(II) and Cr(VI) from aqueous solution. The effect of various parameters like concentration, contact time, and pH of the medium on the adsorption efficiency of the adsorbent was studied. It was found that equilibrium achieved after 20 min while optimum pH for Pb(II) and Cr(VI) was 5 and 3, respectively. The maximum efficiency of the adsorbent ($Q_{max}$) for Pb(II) was 84%, while for Cr(VI) it was 92%. Results demonstrate that Pb(II) and Cr(VI) adsorption onto iron nanoparticles (IONPs) and IONPs/PVA nanocomposites followed the pseudo-second-order kinetics reaction. The adsorption isotherm for Pb was well tailored by the Langmuir adsorption model, while the Cr adsorption was described by the Freundlich adsorption isotherm. The sorption model parameter demonstrates that the synthesized materials can be utilized as an excellent economical nano-adsorbent for removal of Pb(II) and Cr(VI) from water.

*Keywords:* Adsorption; Environmental remediation; Mn-doped iron oxide; PVA nano-composites; Heavy metals

## 1. Introduction

Water is considered as a sign of life on earth as well as human health greatly depends upon the quality of water i.e. purity. Unfortunately, the advent of industrialization and excessive urbanization has degraded the quality of water [1,2]. These two factors contribute much to the accumulation of heavy metals in waters, thus causing water pollution, and heavy metals contamination is a big concern for the whole world especially in developing countries [3,4].

* Corresponding author.

According to the United State of America's Environmental Pollution Agency, the presence of heavy metals, even in lower concentrations in water resources is harmful to human health and can cause severe complications like hepatitis, anemia, nephropathy, and encephalopathy [5]. Like other metals, lead(II) and chromium(VI) are two potent hazardous metals causing complications like damage to respiratory and digestive systems, skin, hepatic disorders, learning difficulties in children, and cancer in humans [6]. According to the WHO guidelines, the allowed concentration of Pb(II) and Cr(VI) is 0.01 and 0.05 mg/L, respectively [7,8]. These heavy metals enter into the water bodies via soil erosion, mining, sewage discharge, industrial effluent, use of pesticides, herbicides, antibiotics, and fertilizers [9,10] and thus disrupt the natural environment which seriously affects the living organism.

Thus, the safe disposal, management, and removal of these fetal heavy metals are of utmost importance. Different techniques such as chemical coagulants, photo-catalytic oxidation, ion exchange resins, and adsorption were employed to remove heavy metals from water [11,12]. But drawbacks like the formation of slug, use of excessive chemicals, time consuming, high cost, and low efficiency are associated with these methods, while the adsorption method is free from these complications [13]. Keeping in view these drawbacks of conventional methods, the adsorption process for the removal of heavy metals is considered as best. In this connection, various adsorbents like chitosan, zeolite, clay, fly ash geopolymers, and the most promising one activated carbon have been using for decades. But sometimes these adsorbents do not give desirable results because of low and insufficient efficiency and adsorption capacity [14,15]. This low efficiency problem is greatly solved by the advent of nanotechnology. This field of science concerns the fabrication of material at the nanoscale. These nanomaterials have special properties as compared to their bulk counterpart [16,17]. The application of nanomaterials for the purpose of water purification has got much attention as compared to other methods. Chitosan-piperazine composite nanofiltration membranes are used for the desalination of brackish water [18]. As compared to other metallic or nonmetallic nanomaterials, iron oxides based nanomaterials are more efficient in the removal of heavy metals from water due to their magnetic properties [19,20]. This magnetic property makes it re-usable, thus leading to a reduction in the overall cost of the process [21]. Interestingly, this magnetic, and other properties like electrical and optical behavior, can be enhanced to a greater extent by the addition of another metal like cobalt and manganese as a dopant. However, in this case, selection of dopant and method are of great importance [22,23]. Some composites of organic materials having special functional groups and ligands are also used for the detection and removal of heavy metal ions from wastewater showing good results at a very low level of the contaminants. However, high cost and pH sensitivity of these organic composites reduce the practical applicability of these materials [24]. Similarly, with all remarkable properties associated with the nanoparticles, the chance of agglomeration always exists. In this context, the development of composites consists of nanoparticles and suitable organic polymer like polyvinyl alcohol (PVA) is a better option [25]. Various functional groups associated with the organic polymer also play a crucial role in the removal of metal ions from the media [26] and the presence of magnetic iron oxide enables it to recover the composite and reuse it [27]. Recycling of the nanocomposites after first cycle with good stability is reported while the recyclability of the nanoparticles alone is still ambiguous [28]. Iron oxide nanoparticles and their composites are synthesized by different methods like thermal decomposition, co-precipitation, and sono-chemical [29,30]. However, co-precipitation method is preferred mostly [31].

Iron oxide nanoparticles synthesized through chemical methods are highly crystalline and uniform, but the use of hazardous chemicals makes these methods lest suitable for environmental prospective.

The basic aim behind the plant mediated synthesis is to avoid the use of toxic chemicals, thus minimizing the chance of any adverse effect on the environment. At the same time, the green method has many other advantages over the chemical and physical methods, such as low energy consumption and avoiding the use of toxic chemicals to save the environment [32,33].

Biosynthesis of nanoparticles are bottom–up approach. The plant extracts contain antioxidants, which have a strong reducing capability and are responsible for the reduction of metal salts to their respective nanoparticles [34]. However, quite limited work has been reported for the green synthesis of iron oxide nanoparticles. There are only some reports available for the synthesis of amorphous iron, hexagonal metallic iron, and $\alpha$-$Fe_2O_3$ nanoparticles using an extract of tea [35] and *Sorghum bran* [36] as reducing agents.

Iron oxide nanoparticles synthesized via tea extract were found nontoxic when compared with the iron oxide nanoparticles synthesized using the conventional $NaBH_4$ reduction protocol. The concentration of tea extract in the reaction mixture plays an important role in controlling the size and crystallinity of the synthesized nanoparticles [37].

*Zanthoxylum armatum* (Z. *armatum*) is an important medicinal plant that belongs to the family Rutaceae. It is widely distributed in different areas of Pakistan, China, India, Nepal, and Japan at an altitude of 1,300–1,500 m [38]. Here we used leaf extract of *Z. armatum* as reducing as well as capping agents in the synthesis of iron oxide nanoparticles. Phytochemical study of *Z. armatum* revealed that various types of alkaloids, lignins, flavonoids, sterols, and terpenes are present in their leave's extract [39]. Polyvinyl alcohol/PVA is a polymer that has good biocompatibility, non-toxicity, excellent mechanical strength, thermal as well as pH stability, and low cost. Composites of PVA with gelatin have been synthesized and employed for the removal of Pb(II), similarly, the composites of PVA/gelatin/SPION have been designed and used for the removal of Cu(II) and Zn(II) [40]. Here in this project, we present the synthesis of PVA and manganese doped iron oxide nanocomposites via green synthesis for the first time.

## 2. Experimental setup

### 2.1. Materials and methods

Fresh plant leaves of *Z. armatum* were collected from district Mansehra, KP Pakistan. Ferrous chloride tetra-hydrate

($FeCl_2 \cdot 4H_2O$) and ferric chloride hexa-hydrate ($FeCl_3 \cdot 6H_2O$) salts were used as precursors; hydrazine hydrate was added to adjust the pH. Polyvinyl alcohol used as a matrix for the preparation of nanocomposites materials. All analytical grade chemicals were purchased from BDH UK and were used without further purification.

### 2.2. Synthesis of nanoparticles

For the synthesis of IONPs, a simple, eco-friendly, and inexpensive co-precipitation method was used [41]. Briefly, 0.5 M solution of ferrous and ferric chloride were prepared separately. These two solutions were mixed in 1:2 ratios by volume up to 150 mL. To this mixture, 10 mL a fresh aqueous plant extract was added, followed by the drop wise addition of hydrazine hydrate in order to keep the pH between 8 and 12 [42]. The reaction mixture was stirred and heated on a hot plate by keeping the temperature at 70°C resulting in the formation of a precipitate. After 30 min, the precipitate was collected by centrifugation (9,000 rpm) and then dried in an oven at 80°C for 4 h. The resulting product was calcined at 500°C for 4 h. For the synthesis of doped iron oxide nanoparticles, Manganese sulfate solutions with different concentrations were added to the ferric and ferrous chloride solution before the addition of plant extract while the remaining conditions and parameters were kept same.

### 2.3. Nanocomposites fabrication

For the synthesis of nanocomposites, 5 g PVA was dissolved in deionized water to make a 5 wt.% solution. In this prepared PVA solution, 0.5 g of undoped iron oxide nanoparticles were dispersed and stirred the mixture on a magnetic stirrer for 1 h in order to get a uniform mixture. The mixture was cast in polystyrene made petri dishes to obtain thin films of iron oxide/PVA nanocomposites. These Petri dishes containing iron oxide/PVA nanocomposites were kept at 60°C in the oven for 7 h for drying. The procedure was repeated for the preparation of manganese doped iron oxide nanoparticles/PVA composites thin films separately. The films were applied for characterization and desalination.

### 2.4. Characterizations

The presence of the optical properties of the nanomaterials was studied with the help of UV-visible spectrophotometer (UV-1800) Shimadzu, Japan, at room temperature in the range of 700–200 nm. The metallic bond that exists between Fe and O and the presence of various functional groups was studied with the help of an FTIR spectrophotometer. The IR spectrum was recorded on Shimadzu IR Affinity-1S Japan; in 500–4,000 $cm^{-1}$ spectral range. The nature of the crystal and average crystal size of the prepared samples were measured by XRD (PanalyticalX'Pert Pro) Netherland; with cobalt as a source. Surface morphology, the elemental analyses, and agglomeration behavior of the samples were studied using (Philips CM12/STEM electron microscopy, PW6030 (120 kv) Hitachi, Japan. The analyses of Cr(VI) and Pb(II) ions in water before and after treatment with IONPs and nanocomposites were done with an Agilent 7700× ICP-MS instrument.

### 2.5. Heavy metals removal

Heavy metal analysis was carried out using inductive coupled plasma mass spectrometry (Agilent 7700× ICP-MS). The contaminated aqueous stock solution was artificially prepared (1 ppm) by adding metal (lead acetate) in deionized water. Similarly, another stock solution was artificially prepared (1 ppm) by adding metal chromium nitrate into deionized water. In five polytetrafluoroethylene tubes, 10 mL lead acetate solution was added, while in other tubes, 10 mL of chromium nitrate solution was added. To each polytetrafluoroethylene tube of lead acetate solution and chromium nitrate solution 0.3 g adsorbents (pure IONPS, 5% Mn doped IONPS, pure IONPS/PVA, and 5% Mn doped IONPS/PVA nanocomposites) were added, and one was kept as such for standard. These tubes were kept on orbital shaker for 1 h. The absorbents were then filtered and the filtrate was analyzed through inductive coupled plasma mass spectrometer for unabsorbed lead and chromium metals. The concentrations of the heavy metals were determined before and after treatment with nanoparticles and nanocomposites and the percent removal (%) was calculated by the following equation:

$$\text{Removal}\left(\%\right) = \frac{C_0 - C_e}{C_0} \times 100 \tag{1}$$

where $C_0$ is the initial concentration, while $C_e$ is the concentration at equilibrium after treatment with nanoparticles and nanocomposites.

### 2.6. Isotherm methodology

The number of heavy metals ($q$) adsorbed per unit mass of adsorbent can be calculated with the following equation.

$$q = \frac{C_i - C_f}{w_t} \times V \tag{2}$$

where $C_i$ is an initial concentration in (mg/L) of heavy metal, $C_f$ is a final concentration in (mg/L) of heavy metal at equilibrium, $V$ is the volume of solution (L), and $w_t$ is the adsorbent dosage (g). The sample was taken at regular time intervals and the heavy metal ions concentration was measured to find out kinetics of the process. The amount of metal ions $q_t$ (mg/g) at time $t$, for lead(II) and chromium(VI) adsorbed by $Fe_2O_3$ nanoparticles and $Fe_2O_3$/PVA nanocomposites, was calculated through Eq. (3):

$$q_t = \frac{C_0 - C_t}{w_t} \times V \tag{3}$$

To find the isotherm models and the kinetic rate equation that the adsorption process will follow, the values of $C_f$, $C_t$, $q$, and $q_t$ are used in the above equations.

*2.6.1. Langmiur isotherm*

The Langmiur theory gives information about the adsorption of gases on metal surfaces and also has applications in other adsorption processes. Langmuir's model says that as the distance increases, the intermolecular forces decrease rapidly, which shows the presence of a single layer of adsorbate at the exterior of the adsorbent. Further, the isotherm equation undertakes that adsorption occurs at definite identical sites of the adsorbent. Hence, it is concluded that once a Pb(II) ions or Cr(VI) occupies a site, that site becomes locked.

The linear form of isotherm is represented as follows:

$$\frac{C_e}{q_e} = \frac{1}{Q^0 b} + \frac{1}{Q^0} C_e \tag{4}$$

In the Eq. (4) $Q^0$, is metal ion uptake per unit mass of adsorbent (mg/g) and $b$ is a constant called Langmuir constant. Therefore, $C_e/q_e$ vs. $C_e$ provides a straight line with slope $1/Q^0$ and intercept $1/(Q^0 b)$.

*2.6.2. Freundlich adsorption isotherm*

The Freundlich isotherm is applicable to non-ideal adsorption that involves the adsorption of different phases. Freundlich isotherm is represented by Eq. (5) as:

$$q_e = K_F C_e^{\frac{1}{n}} \tag{5}$$

The equation is accessibly used in the linear form by taking the logarithm of both sides as:

$$\log q_e = \log K_F + \frac{1}{n} \log C_e \tag{6}$$

Freundlich constants $K_F$ relates to adsorption capacity while $1/n$ to the passion of adsorption. The slope and intercept of the plot ($\log q_e$ vs. $\log C_e$) from the above equation give the values of $n$ and $K_F$. Freundlich isotherm explains the affiliation among equivalent adsorption capacity, $q_e$ (mg/g), and the amount of metal ions in solution at equilibrium $C_e$ (mg/L). The plot of $\log(q_e)$ vs. $\log(C_e)$ was found to be linear for many initial concentrations.

*2.7. Kinetic study*

*2.7.1. Kinetic-first-order rate equation*

The pseudo-first-order equation in linear form is given as:

$$\log\left(q_e - q_t\right) = \log q_e - \frac{k_1}{2.303} t \tag{7}$$

where $q_t$ and $q_e$ (mg/g) are the quantities of lead(II) or chromium(VI) adsorbed at equilibrium by time $t$ (min), and $k_1$ (1/min) is the rate constant. The values of $\log(q_e - q_t)$ were derived from the kinetic data and plotted against time ($t$).

*2.7.2. Kinetic second order rate equation*

Following is the pseudo-second-order rate equation:

$$\frac{t}{q_t} = \frac{1}{k_2} \times \frac{1}{q_e^2} + \frac{1}{q_e} t \tag{8}$$

where $q_t$ and $q_e$ are the quantity of lead(II) or else chromium(VI) adsorbed (mg/g) at equilibrium and time $t$ (min), $k_2$ (g/mg min) is pseudo-second-order rate constant. Standards of $t/q_t$ were calculated from the kinetic data and plotted against time ($t$).

*2.7.3. Effect of pH*

The effect of pH on the adsorption of Cr(VI) and Pd(II), we selected pH in between 2 and 7, the pH was adjusted by the controlled addition of 0.1 M HCl or 0.1 M NaOH solution as needed and monitored by pH meter. The remaining parameters were kept constant.

*2.8. Reusability study*

The selective adsorption of Cr(VI) removal by prepared nanocomposites is high as compared to Pb(II). Thus, Cr(VI) was selected for further detailed reusability study. The reusability of the pure, Mn doped IONPs, and IONPs/PVA composites was investigated for the removal of Cr(VI) for five reaction runs. Reusability of composite was studied by mixing 20 mg of Cr(VI) ions-loaded composite into 10 mL of 0.1 M HCl solution and sonicating for 5 min. Then, the washed composite was separated from the solution by a Whatman filter paper 42, and washed with distilled water three times, and dried for reuse on the same day.

## 3. Results and discussion

*3.1. UV-visible analysis*

The iron oxide nanoparticles, both pure and doped with manganese prepared via the co-precipitation method, were examined by a UV-visible spectrophotometer. Pure metals and metal nanoparticles are unique from other nanoplatforms by their characteristic surface plasmon resonance (SPR). This SPR is the collective oscillation of the surface electrons of nanoparticles. The solution mixture was monitored and analyzing using UV-visible spectrophotometer with a wavelength range of 200–700 nm. The UV-visible spectra of pure and Mn doped nanoparticles are shown in Fig. 1. From the literature survey, iron oxide nanoparticles typically show maximum absorbance in the range of 300–450 nm, which is attributed to the scattering and absorbance of light by magnetic nanoparticles. In the present work, the nanoparticles show absorbance between 370 and 400 nm. It has been reported in the literature that *Punica granatum* mediated iron oxide nanoparticles showed surface Plasmon resonance at 375 nm [43], which is closely related to our result. The maximum absorbance is at 380 nm and there is a slight increase in the absorption maxima with doping of nanoparticles. The increase in the absorbance maxima may be due to the increase in the

ionic radii of $Mn^{2+}$ ion than $Fe^{3+}$ [44]. These results show that prepared nanoparticles were synthesized successfully, adopting a green approach as compared to other chemical methods which are based on the use of toxic reagents. The surface chemistry of biosynthesized nanoparticles have a diverse range of biomolecule such as flavonoids, phenols, proteins, tannins, and amino acids that are the supporting units IONPs. The SPR of the biosynthesized nanoparticles tends to gain the capping agent biomolecules of the extract and attract them, by giving different surface chemistry that is purely being supported by reducing molecules of the plants.

### 3.2. FT-IR spectroscopy

FT-IR analysis of synthesized pure and Mn doped IONPs was performed for the detection of reducing as well as stabilizing agents of the nanoparticles. FT-IR spectroscopy is a very important tool in the nanotechnology for identification of the organic functional groups present in the extract of plant which are responsible for stabilizing of bio-synthesized nanoparticles. The FTIR spectra of pure iron oxide/PVA nanocomposites and the doped iron oxide/PVA nanocomposites are shown in Fig. 2. In both spectra, the absorption band at 625 $cm^{-1}$ is present, which is assigned to the stretching vibration of the metal-oxygen bond, that is, Fe–O bond, therefore confirming the synthesis of iron oxide nanoparticles [45,46]. As we used plant extracts for stabilization and PVA for composites preparation, other peaks were also observed rather than M–O starching vibration. PVA possesses functional groups like –OH, $–CH_2$, and C–O–C. The peaks observed 3,640 $cm^{-1}$ confirm the –N–H functional group present in the plant extract, the peak at 2,940 $cm^{-1}$ corresponds to the stretching vibration of C–H, while peak at 1,180 $cm^{-1}$ is due to C–O–C stretching vibration [47]. The observed bands at 1,412 $cm^{-1}$ could be assigned to the C–N stretching vibrations mood of aromatic amines [48]. The sharp peak at 1,260 $cm^{-1}$ corresponds to the C–O stretching vibration of carboxylic acids the plant extract [49]. The peak at 2,359 $cm^{-1}$ may be due the adsorption of $CO_2$. If we inspect Fig. 2, we do not observe any peak in the region of 3,200–3,600 $cm^{-1}$ for iron oxide and manganese doped iron oxide nanoparticles because we used PVA only in composite preparation, hence the presence of –OH in the composite while the absence in nanoparticles samples clearly demonstrates the successful synthesis of iron oxide/PVA nanocomposites [40,50].

### 3.3. Surface morphology

In order to find out the morphology, surface, and size of prepared pure and Mn doped IONPs, SEM, and TEM analyses were carried out (Figs. 3–5). It has been reported in the literature that electronic and optical properties of nanomaterials considerably depend upon the size and shape nanoparticles [51]. The structure and morphology of the powder samples of iron oxide nanoparticles and a thin film of $Fe_2O_3$-PVA nanocomposites were studied using SEM. The SEM images show that iron oxide nanoparticles were aggregated, having an irregular shape with rough surfaces. The surface of the nanoparticles seems to be porous and spongy (Fig. 3). The SEM images of $Fe_2O_3$-PVA nanocomposites (both the cross-section and surface) are given in Fig. 4. The SEM images of $Fe_2O_3$-PVA show that nanoparticles are embedded and uniformly distributed in the PVA matrix. SEM results (Fig. 3) show that pure and Mn doped nanocomposites just like similar previously reported *P. granatum* mediated iron oxide nanoparticles [43].

In order to obtain the particle size of nanoparticles, TEM analysis was carried out (Fig. 5). TEM images show that the particles are of spherical and rod shapes. The calculated average size of pure and 5% Mn doped IONPs was 25 and 19 nm, respectively. TEM images showed that the particles are relatively mono-dispersed and are uniformly distributed throughout. TEM result (Fig. 5), showed that pure and Mn doped nanocomposites synthesized by biologically method are different in size because of the different precursor added into the reaction. Furthermore, it is interestingly found that the prepared iron oxide nanocomposites

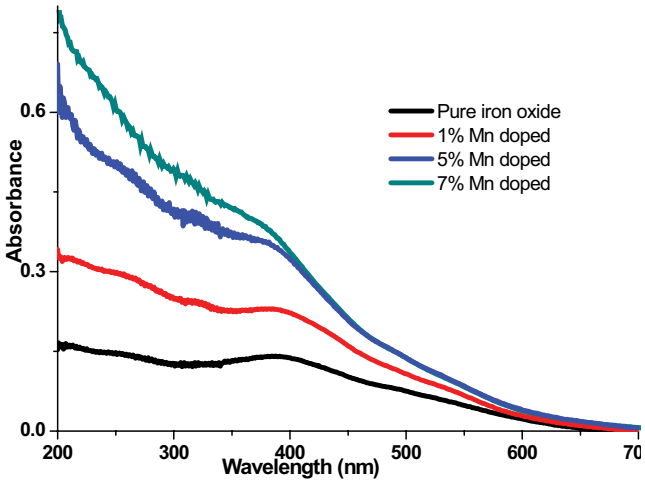


Fig. 1. UV-visible spectra of pure IONP, 1% Mn doped IONP, 5% Mn doped IONPS, and 7% Mn doped IONPS.

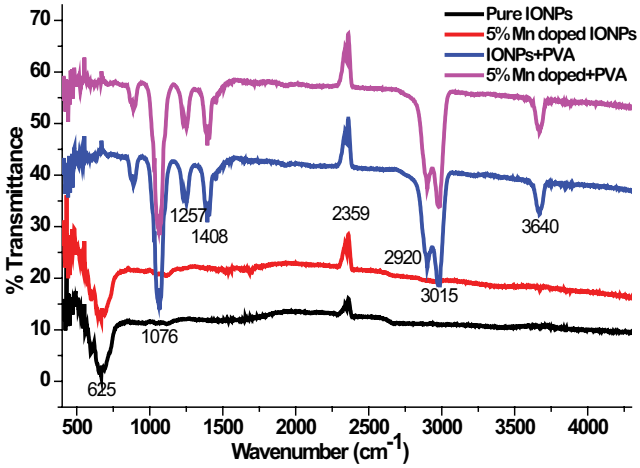


Fig. 2. FT-IR spectra of pure IONP, 5% Mn doped IONP, pure IONPS-PVA nanocomposites, and 5% Mn doped IONPS-PVA nanocomposites.

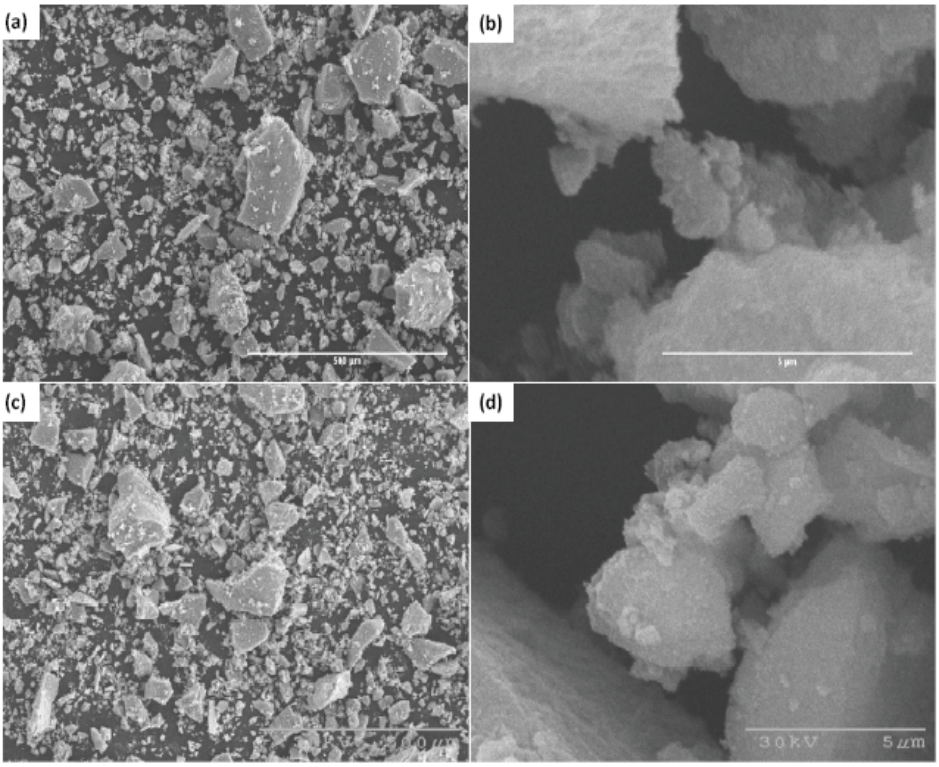


Fig. 3. SEM images of pure IONP and 5% Mn doped IONP ((a and c) 500 μm, (b and d) 5μm).

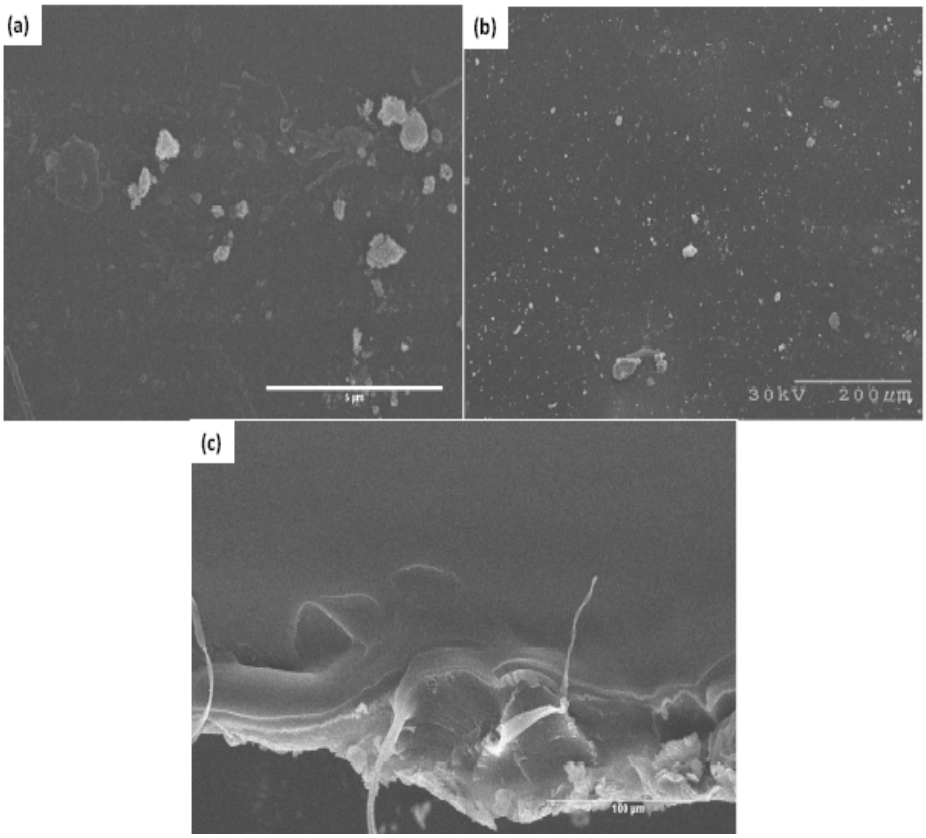


Fig. 4. SEM images of (a) pure IONPS-PVA nanocomposites (5 μm), (b) 5% Mn doped IONPS-PVA nanocomposites (200 μm), and (c) the cross section of pure IONPS-PVA nanocomposites (100 μm).

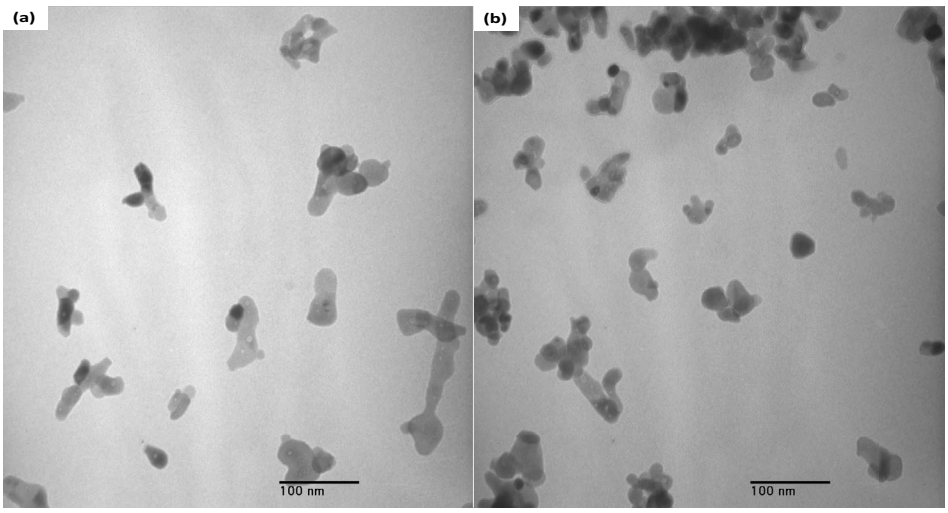


Fig. 5. TEM images of (a) pure IONP and (b) TEM image of 5% Mn doped IONP.

are well-organized and just like similar reported nanorods previously [52].

### 3.4. XRD pattern

The XRD patterns of all four samples, are well defined and intense, confirm the presence of crystallinity in samples, and the major peaks present in all four samples are (220), (104), (110), (311), (113), (400), (024), (116), and (320). All these Bragg peaks are the characteristics of planes of IONPs. A Sherrer's equation was used for the calculation of the average size of the synthesized pure and Mn doped IONPs:

$$L(\text{nm}) = \frac{k\lambda}{\beta_{1/2}\cos\theta} \tag{9}$$

In this Eq. (9) $L$ represents the size of the particle, $k$ is a constant equal to 0.89, $\lambda$ can be used as 0.15432 nm from CuK$\alpha$ radiation source, $\beta_{1/2}$ is the full width at half maximum and 2θ is the diffraction angle. By putting the value into the Scherrer formula together with $\lambda$ = 1.54, $k$ = 0.89, and β was calculated. The calculated average size of crystals were 14.56, 13.4, and 15.26 nm for pure IONPs, 5% Mn doped IONPs and IONP/PVA nanocomposites, respectively. The absence of any oxide peak related to the oxides of Mn suggests successful doping of the host material with $Mn^{2+}$. Beside the absence of manganese related peaks, there is a slight deviation in 2θ and this deviation is only due to the replacement of $Fe^{2+}$ ions by the dopent $Mn^{2+}$ ions [41].

### 3.5. Heavy metals removal efficiency of nanoparticles and nanocomposites

The discharge of heavy metals into the natural environment from different industries is of great concern all over the world. Heavy metals have unpleasant effects on aquatic life, natural environment, and human health. Due to non-biodegradable nature, solubility in water, long biological half-lives, and their potential to accumulate in various parts of the body, heavy metals are extremely harmful.

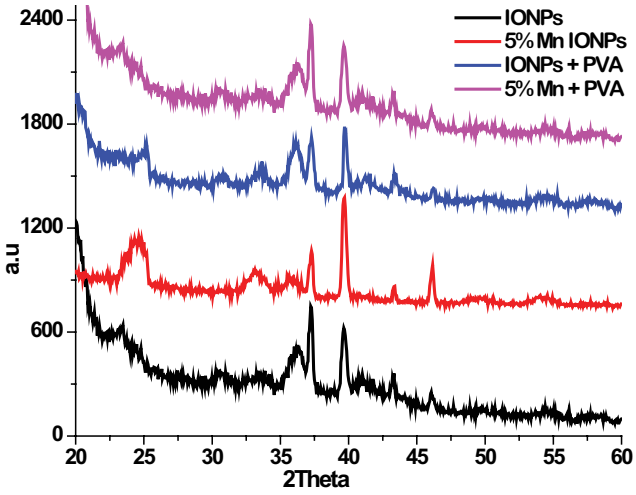


Fig. 6. XRD patterns of pure IONP, 5% Mn doped IONP, pure IONPS-PVA nanocomposites, and 5% Mn doped IONPS-PVA nanocomposites.

During the investigation of heavy metals, the concentration of the heavy metals was determined before and after treatment with nanoparticles and nanocomposites, and the percent removal (%) was calculated. Table 1 and Fig. 7 show the results and other parameters for the lead(II) detection. The results and other parameters of chromium(VI) are shown in Table 2 and Fig. 8.

Now a day the reusability and recyclability of the active catalyst in catalysis is a very significant issue. As the most of catalysts are de-activated after single or second cycle. Beside catalytic activity, stability, reusability, and the photocorrosion are very important parameters for evaluating the catalyst performance as it could significantly decreased the cost of the chemical process. Catalysts in the literature were effectively reported in the form of nanoparticles to show effective photoreduction activity, but the problem is their recyclability for next use. That's why, the simple separation of the catalysts for

Table 1
Parameters and results of IONPs and IONPs/PVA composites for Pb(II)

| S. No | $Fe_{1-x}Mn_x$ | $T$ (°C) | pH | Time (min) | Adsorbent amount (g) | %Removal |
|---|---|---|---|---|---|---|
| 1 | 0% IONPs | 25 | 4 | 180 | 0.05 | 68 |
| 2 | 5% IONPs | 25 | 4 | 180 | 0.05 | 75 |
| 3 | 0% IONPs/PVA composites | 25 | 4 | 180 | 0.05 | 78 |
| 4 | 5% IONPs/PVA composites | 25 | 4 | 180 | 0.05 | 84 |

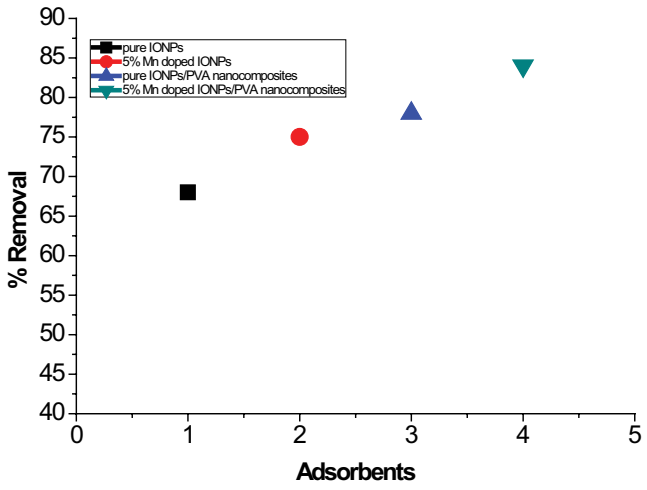


Fig. 7. Percentage age efficiency of IONPs and IONPS/PVA composites in removal of lead.

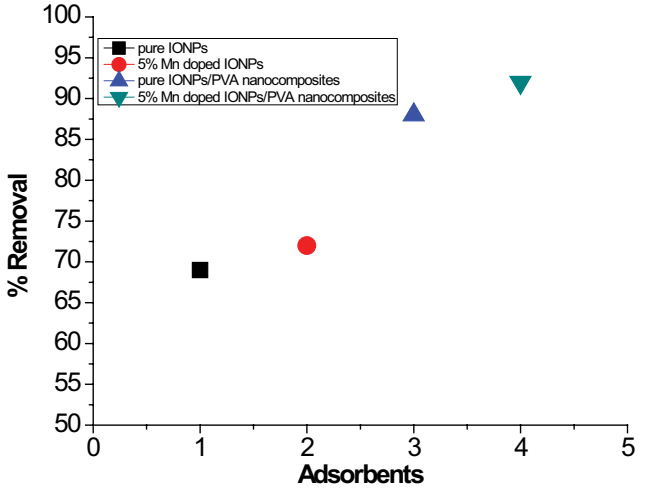


Fig. 8. Percentage age efficiency of IONPs and IONPS/PVA composites in removal of chromium.

reusability purpose is quite important. Here in the currect study pure IONPs, Mn doped IONPs, and IONPs/PVA nanocomposites were study for the reusability of Cr(VI). The results of the reusability is presented in Table 3.

#### 3.5.1. Influence of contact time for Pb(II) removal

To study the equilibrium time for uptake and to find out the kinetics of adsorption, lead adsorption on pure IONPs, 5% Mn doped IONPs, pure IONPs/PVA nanocomposites and 5% Mn doped IONPs/PVA nanocomposites as adsorbents were examined as a function of contact time and fallouts are shown in Fig. 9. Lead(II) was quickly adsorbed by the adsorbents in about 20 min.

The contact was kept for almost 60 min to confirm that equilibrium was indeed achieved as the sample was withdrawn at every ten minutes. It can be observed from Fig. 9 that, in the beginning, the number of active sites is abundant and the removal efficiency is higher. After 20 min, equilibrium is achieved, from which we can calculate the value of $q_e$ as the sorption became less proficient in the later stages.

#### 3.5.2. Influence of contact time for Cr(VI) elimination

Similarly to study the equilibrium time for uptake and to find out the kinetic of adsorption, chromium adsorption on pure IONPs, 5%Mn doped IONPs, pure IONPs/PVA nanocomposites, and 5% Mn doped IONPs/PVA nanocomposites as adsorbents were also examined as a function of contact time and the results are shown in Fig. 10. Chromium was quickly adsorbed by the adsorbents in about 20 min. The contact was kept for about 60 min to confirm that equilibrium was indeed achieved as the sample was withdrawn at every ten minutes. It can be observed from Fig. 10 that

Table 2
Parameters and results of IONPs and IONPs/PVA composites for Cr(VI)

| S. No | $Fe_{1-x}Mn_x$ | $T$ (°C) | pH | Time (min) | Adsorbent amount (g) | %Removal |
|---|---|---|---|---|---|---|
| 1 | 0% IONPs | 25 | 4 | 180 | 0.05 | 69 |
| 2 | 5% IONPs | 25 | 4 | 180 | 0.05 | 72 |
| 3 | 0% IONPs/PVA composites | 25 | 4 | 180 | 0.05 | 88 |
| 4 | 5% IONPs/PVA composites | 25 | 4 | 180 | 0.05 | 92 |

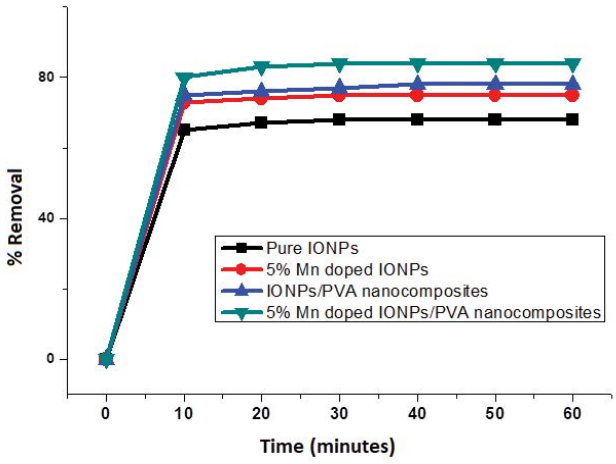


Fig. 9. Percentage removal of lead vs. contact time.

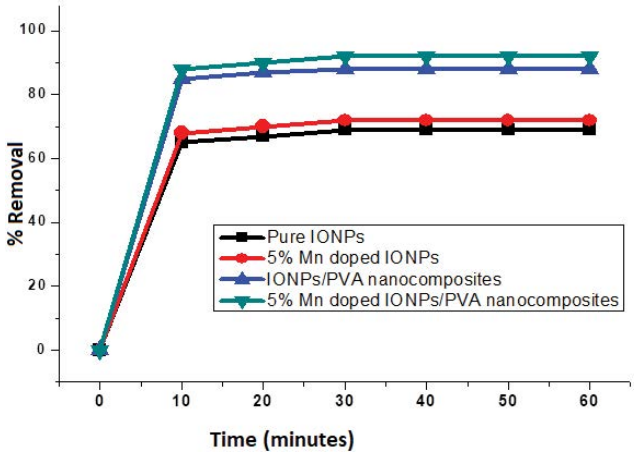


Fig. 10. Percentage removal of chromium vs. contact time.

at the beginning, the number of active sites is abundant and the removal efficiency is high. After 20 min equilibrium is achieved from which we can calculate the value of $q_e$ as the sorption became less effective in the later stages.

### 3.5.3. Effect of pH

The pH of the medium greatly affects the adsorption of metal ions on the surface of the adsorbent, because pH can change the surface's charges of the adsorbent. Similarly, the pH of the medium also affects the adsorbate. The point of zero charges is the condition when the density of electric charge on the surface of the adsorbent is equal to zero. When pH is less than the point of zero charges the surface of adsorbent becomes positively charged thus capturing more anions conversely, when the pH of the medium becomes greater than the point of zero charges, adsorbent surface becomes negatively charged thus attracting the cations [53]. In the present work, the effect of pH on the adsorption of Cr(VI) and Pd(II) has shown in Figs. 11 and 12, respectively. Keeping other factors like temperature, adsorbent amount, and initial concentration of Cr(VI) constant, the adsorption was maximum in the range of pH 2–3. However, maximum adsorption was achieved at pH 3, after that when pH increased slowly up to seven adsorptions decreased gradually. In this rang of pH Cr(VI) exists in $HCrO_4^-$ or $CrO_2^-$ form in the medium. At lower pH, that is, 2 and 3 $HCrO_4^-$ dominate over $CrO_2^-$ hence adsorption is maximized, and when the pH shift toward seven adsorptions gradually decreases because competition between $CrO_2^-$ and $OH^-$ increase as result adsorption of target metal ions decrease. In this work the same situation exists, adsorption is higher at pH 2 which increased further at pH 3 however, after that we observe a slow and steady decrease in adsorption. The adsorbent surface bear $–NH_2$ group as depicted in FTIR analysis, this group converts in $NH_3^+$ which is the cause of high adsorption of Cr(VI) at pH 3 [25,54]. Similarly, for Pb(II), the same situation was observed like Cr(VI), adsorption increases slowly when the pH increases from 2 to 5 however beyond 5 it decreases again. At a lower pH density of $–NH_2$ groups are low, hence the adsorption of Pb(II) was low. On the other hand, adsorption again decreased when the pH increased from 5 to 7 this decrease was due to the formation of hydroxides which also hinder the adsorption. So in the present work, adsorption of Cr(VI) and Pb(II) was maximum at pH 3 and 5, respectively, hence marking values as an optimum pH value [14].

### 3.6. Modeling of adsorption isotherms

According to the Langmuir isotherm, the curiosity arises on the surface of the same phase by single layer sorption deprived of interaction between adsorbed ions.

The linear form of the Langmuir isotherm equation is:

$$\frac{C_e}{q_e} = \frac{1}{Q^0 b} + \frac{1}{Q^0} C_e \tag{10}$$

where $Q^0$ is the maximum metal ion endorsement per unit mass of adsorbent (mg/g) and $b$ is the Langmuir constant. A plot of $C_e/q_e$ vs. $C_e$ provides a straight line of slope $1/Q^0$ and intercept $1/(Q^0 b)$ [55,56].

Table 3
Langmuir adsorption isotherm constants and parameters for Pb(II)

| Adsorbent | $Q_{max}$ (mg/g) | $b$ | $R_L$ | $R^2$ |
|---|---|---|---|---|
| Undoped IONPs | 21.54 | 0.63 | 0.19 | 0.992 |
| 5% Mn doped IONPs | 27.89 | 0.65 | 0.21 | 0.994 |
| Undoped IONPs/PVA nanocomposites | 23.45 | 0.64 | 0.20 | 0.992 |
| 5% Mn doped IONPs /PVA nanocomposites | 34.77 | 0.71 | 0.24 | 0.997 |

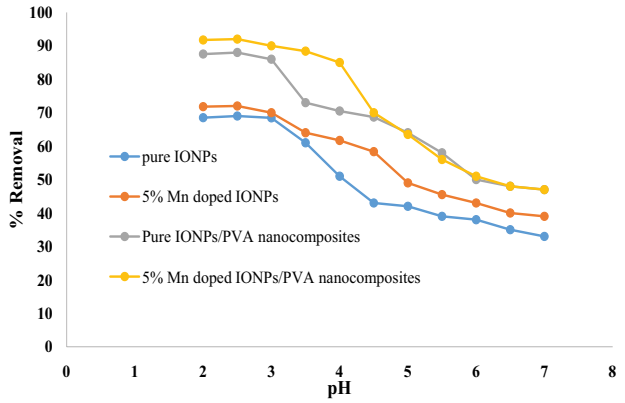


Fig. 11. Effect of pH on removal of Cr(VI).

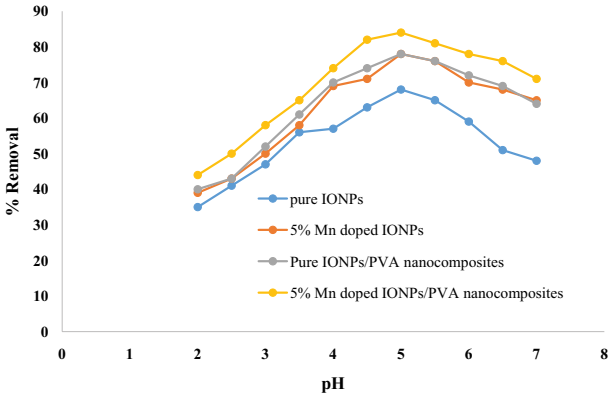


Fig. 12. Effect of pH on removal of Pb(II).

Table 4
Freundlich adsorption isotherm constants and parameters for Cr(VI)

| IONPs | $n$ | $R^2$ | $K_F$ |
|---|---|---|---|
| Undoped IONPs | 0.54 | 0.991 | 8.78 |
| 5% Mn doped IONPs | 0.48 | 0.996 | 15.77 |
| Undoped IONPs/PVA nanocomposites | 0.47 | 0.997 | 19.24 |
| 5% Mn doped IONPs/PVA nanocomposites | 0.36 | 0.998 | 24.56 |

The Freundlich isotherm is relevant to non-ideal adsorption involving heterogeneous adsorption. Representation of the Freundlich isotherm is:

$$q_e = K_F C_e^{\frac{1}{n}} \tag{11}$$

By taking the logarithm of both sides the equation became:

$$\log q_e = \log K_F + \frac{1}{n}\log C_e \tag{12}$$

The Freundlich constants $K_F$ relates to adsorption capacity, while $1/n$ to the strength of adsorption. Standards of $n$ and $K_F$ can find out from the slope and intercept of the plot $\log q_e$ vs. $\log C_e$ derived from the above equation.

The same set of experimental data was used to check the applicability of the Freundlich and Langmuir adsorption isotherms [57,58].

According to the Langmuir isotherm, the curiosity arises on the surface of the same phase by single layer sorption deprived of interaction between adsorbed ions.

The linear form of the Langmuir isotherm equation is:

$$\frac{C_e}{q_e} = \frac{1}{Q^0 b} + \frac{1}{Q^0} C_e \tag{13}$$

where $Q^0$ is the maximum metal ion endorsement per unit mass of adsorbent (mg/g) and $b$ is the Langmuir constant. A plot of $C_e/q_e$ vs. $C_e$ provides a straight line of slope $1/Q^0$ and intercept $1/(Q^0 b)$ [55,56]. Constants like $b$, $R_L$, $R^2$, and $Q_{max}$ for the Langmuir adsorption isotherm has displayed in Table 5. From the Table 5, it is clearly indicated that $Q_{max}$ increases with the introduction of dopent. Similarly, the feasibility or favorability of the process can be obtained from Eq. (14).

$$R_L = 1/1 + K_L C_0 \tag{14}$$

where $R_L$ is the equilibrium parameter and tells whether the process is favorable or not, such as when $R_L > 1$ the process will be unfavorable, when $R_L = 1$ linear and when $0 < R_L < 1$ the process will be favorable [59]. In the present work, the $R_L$ for all four samples is between 0 and 1 confirming the favorability of the process. Similarly, correlation coefficient $R^2$ is close to unity for Pb(II) in the case of Langmuir adsorption isotherm while for Cr(VI) in the case of the Freundlich adsorption isotherm. $K_F$ and $n$ calculated from the graph plotted between $\ln q_e$ vs. $\ln C_e$. The obtained data well fit in Langmuir and Freundlich modals as well as to satisfy the value of $R_L$ confirming the feasibility of the process. The comparison of $Q_{max}$ of the present work with $Q_{max}$ of already published work available in the literature confirm the suitability and practical utility of iron oxide/PVA nanocomposites.

### 3.7. Kinetic modeling

#### 3.7.1. Pseudo-first-order equation

The adsorption kinetics were fitted into a pseudo-first-order kinetics model, revealing the adsorption rate. The linear form of the equation is:

$$\log\left(q_e - q_t\right) = \log q_e - \frac{K_1}{2.303} t \tag{15}$$

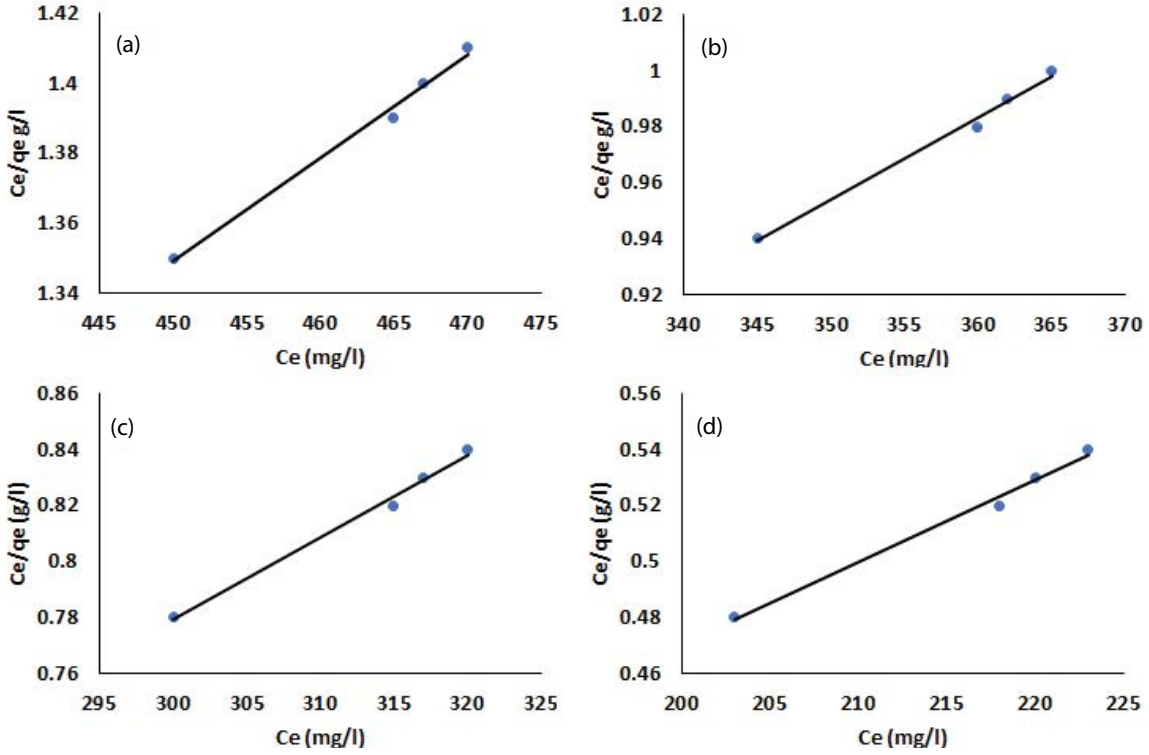


Fig. 13. Langmiur isotherm of lead for (a) pure IONPs, (b) 5% Mn doped IONPs, (c) for pure IONPs/PVA nanocomposites, and (d) for 5% Mn doped IONPs/PVA nanocomposites.

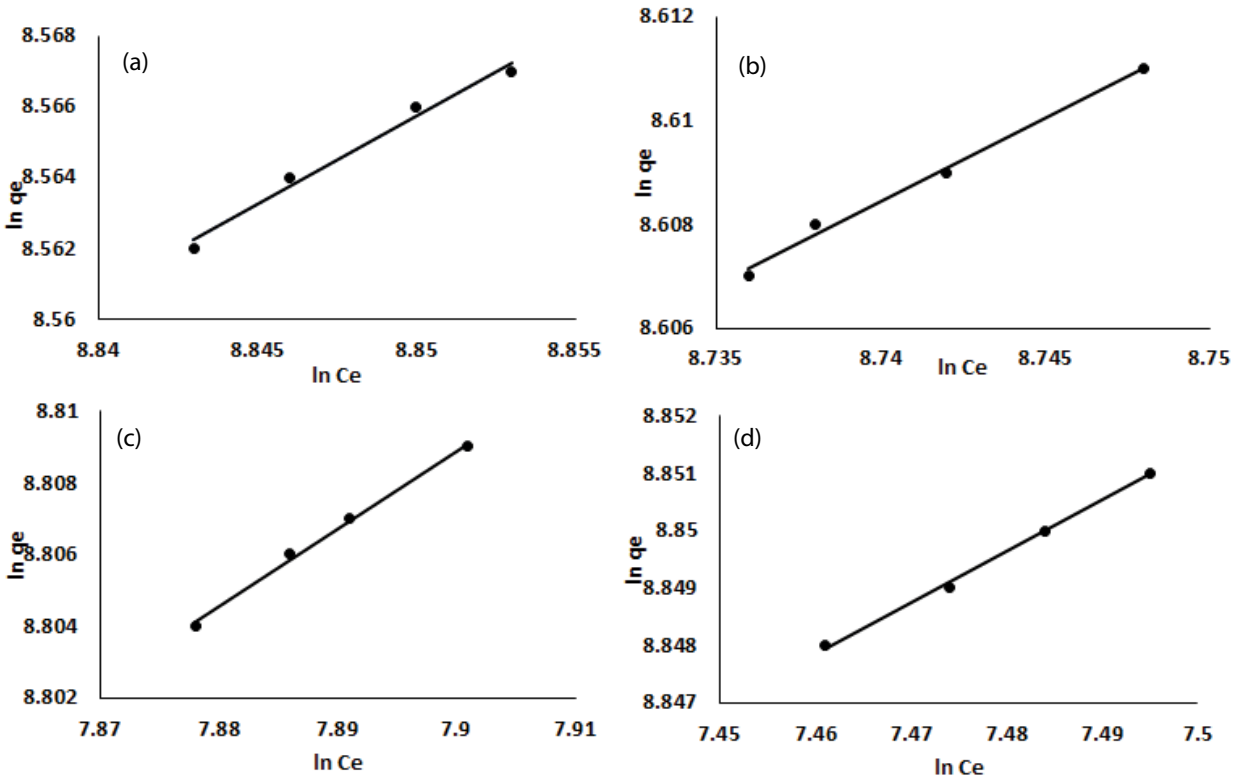


Fig. 14. Fruendlich isotherm of chromium for (a) pure IONPs, (b) 5% Mn doped IONPs, (c) for pure IONPs/PVA nanocomposites, and (d) for 5% Mn doped IONPs/PVA nanocomposites.

Table 5
Comparison of $Q_{max}$ of the present work with published work [60–63]

| Adsorbent | $Q_{max}$ (mg/g) | Reference |
|---|---|---|
| Undoped IONPs | 21.54 | Present work |
| 5% Mn doped IONPs | 27.89 | Present work |
| Undoped IONPs/PVA nanocomposites | 23.45 | Present work |
| 5% Mn doped IONPs/PVA nanocomposites | 34.77 | Present work |
| Magnetic hydrogel beads | 17.66 | [52] |
| Wool graft polyacrylamidoxime | 23.56 | [53] |
| Titanium(IV) oxide nanoparticles | 12.94 | [54] |
| Amino modified $Fe_3O_4$ nanoparticles | 11.24 | [55] |

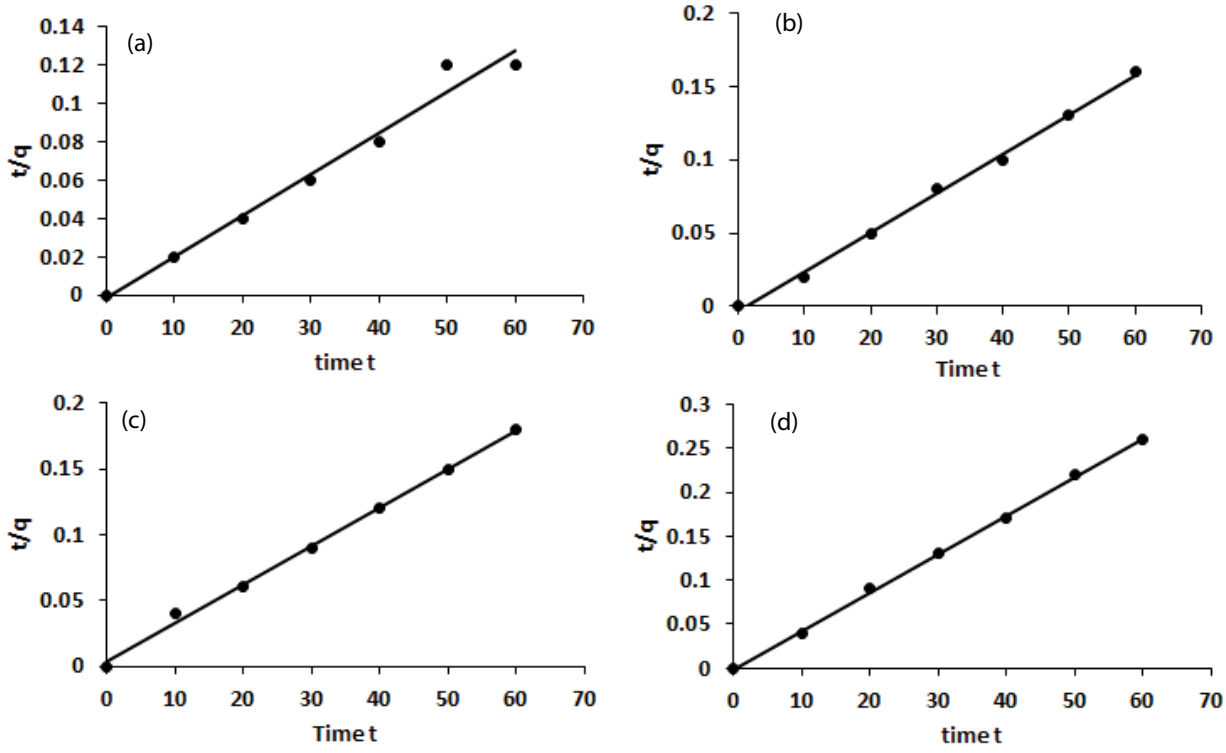


Fig. 15. Second-order-kinetics of (a) pure IONPs, (b) 5% Mn doped IONPs, (c) pure IONPs/PVA nanocomposites, and (d) 5% Mn doped IONPs/PVA nanocomposites for lead.

To obtain rate constant, values of $\log(q_e - q_t)$ were linearly allied through $t$ by plotting the $\log(q_e - q_t)$ vs. $t$. $K_1$ and $q_e$ can be calculated as of the slope and the intercept of the plot.

*3.7.2. Pseudo-second-order equation*

The kinetics of adsorption can be fitted by the pseudo-second-order equation.

$$\frac{t}{q_t} = \frac{1}{K_2} \times \frac{1}{q_e^2} + \frac{1}{q_e} t \tag{16}$$

If the plot of $t/q_t$ vs. $t$ displays a linear relationship, then the second-order kinetics are valid. $K_2$ and $q_e$ values were calculated from the intercept and the slope of the plot $t/q_t$ vs. $t$. The results for adsorption of lead (Pb) and chromium (Cr) onto pure IONPs, 5% Mn doped IONPs, pure IONPs/ PVA, and 5% Mn doped IONPs/PVA are shown in Figs. 15 and 16.

## 4. Conclusions

Nano-science and engineering provide new openings to develop environmentally friendly and cost-effective water treatment technologies. The combination of the co-precipitation method and plant extract of *Z. armatum* could be used for the synthesis of pure and Mn-doped IONPs, as well as their nanocomposites with PVA. After successful synthesis, these nanomaterials were applied for the removal

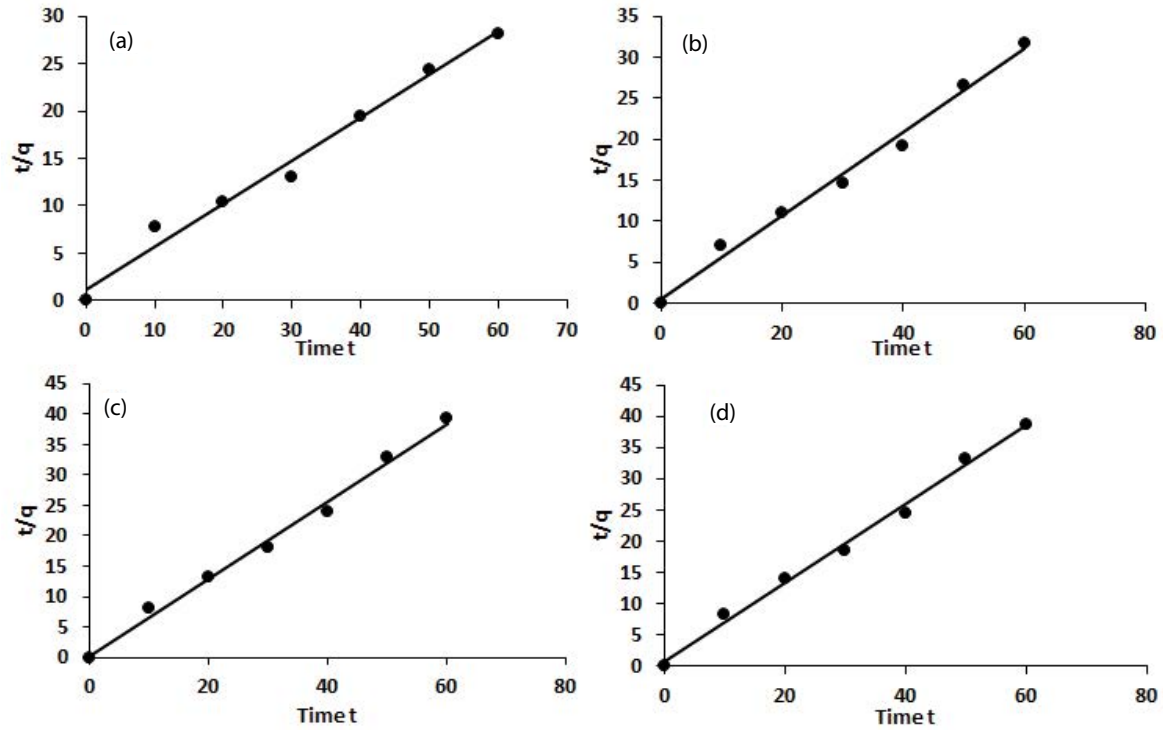


Fig. 16. Second-order-kinetics of (a) pure IONPs, (b) 5% Mn doped IONPs, (c) pure IONPs/PVA nanocomposites, and (d) 5% Mn doped IONPs/PVA nanocomposites for chromium.

of lead(II) and chromium(VI) ions. The adsorption was very fast and equilibrium was achieved within 30 min for both ions. At the same time, the adsorption was highly dependent on pH, and the adsorption was maximum at pH 5 and 3. Adsorption isotherms (i.e., Langmuir and Freundlich) were applied to fit the data, the case of Cr(VI) follows the Freundlich adsorption isotherm while Pb(II) follows the Langmuir adsorption model, and from the kinetic study, it is evident that the process follows pseudo-second-order kinetics instead of the first order. Among the results, the most promising one in the current study is that efficiency is improved with doping. Therefore, nano adsorbent based on the pure, doped IONPs and their composites with PVA is recommended as a fast, inexpensive, and eco-friendly adsorbent for the removal of chromium(VI) and lead(II) ions.

## Acknowledgments

This study is based on Ph.D. research work conducted by Mr. Zahid Wahab as part of his Ph.D. thesis under the supervision of Prof. Dr. Muhsin Nawaz, Department of Chemistry, Hazara University Mansehra, Khyber Pakhtunkhwa, Pakistan. The authors are thankful to the Higher Education Commission (HEC), Pakistan for the NRPU Project No. 5358 financial assistance.

## References

[1] R.P. Schwarzenbach, T. Egli, T.B. Hofstetter, U. Von Gunten, B. Wehrli, Global water pollution and human health, Ann. Rev. Environ. Resour., 35 (2010) 109–136.

[2] M. Bilal, S. Khan, J. Ali, M. Ismail, M.I. Khan, A.M. Asiri, S.B. Khan, Biosynthesized silver supported catalysts for disinfection of *Escherichia coli* and organic pollutant from drinking water, J. Mol. Liq., 281 (2019) 295–306.

[3] M. Fujita, Y. Ide, D. Sato, P.S. Kench, Y. Kuwahara, H. Yokoki, H. Kayanne, Heavy metal contamination of coastal lagoon sediments: Fongafale Islet, Funafuti Atoll, Tuvalu, Chemosphere, 95 (2014) 628–634.

[4] M. Ismail, K. Akhtar, M. Khan, T. Kamal, M.A. Khan, A.M. Asiri, J. Seo, S.B. Khan, Pollution, toxicity and carcinogenicity of organic dyes and their catalytic bio-remediation, Curr. Pharm. Des., 25 (2019) 3645–3663.

[5] M.-W. Wan, C.-C. Kan, B.D. Rogel, M.L.P. Dalida, Adsorption of copper(II) and lead(II) ions from aqueous solution on chitosan-coated sand, Carbohydr. Polym., 80 (2010) 891–899.

[6] Y. Yang, H. Liu, X.-h. Xiang, F.-y. Liu, Outline of occupational chromium poisoning in China, Bull. Environ. Contam. Toxicol., 90 (2013) 742–749.

[7] P. Karrari, O. Mehrpour, M. Abdollahi, A systematic review on status of lead pollution and toxicity in Iran, guidance for preventive measures, DARU J. Pharm. Sci., 20 (2012) 1–17.

[8] V. Velma, S. Vutukuru, P.B. Tchounwou, Ecotoxicology of hexavalent chromium in freshwater fish: a critical review, Rev. Environ. Health, 24 (2009) 129–146.

[9] S. Morais, F.G. Costa, M.d.L. Pereira, Heavy Metals and Human Health, J. Oosthuizen, Ed., Environmental Health–Emerging Issues and Practice, Vol. 10, IntechOpen, 2012, pp. 227–246. Available at: https://www.intechopen.com/books/environmental-health-emerging-issues-and-practice/heavy-metals-and-human-health

[10] S. Xia, Z. Song, P. Jeyakumar, S.M. Shaheen, J. Rinklebe, Y.S. Ok, N. Bolan, H. Wang, A critical review on bioremediation technologies for Cr(VI)-contaminated soils and wastewater, Crit. Rev. Environ. Sci. Technol., 49 (2019) 1027–1078.

[11] F.L. Fu, Q. Wang, Removal of heavy metal ions from wastewaters: a review, J. Environ. Manage., 92 (2011) 407–418.

[12] M.A. Hashim, S. Mukhopadhyay, J.N. Sahu, B. Sengupta, Remediation technologies for heavy metal contaminated groundwater, J. Environ. Manage., 92 (2011) 2355–2388.
[13] K.H. Hassan, E.R. Mahdi, Synthesis and characterization of copper, iron oxide nanoparticles used to remove lead from aquous solution, Asian J. Appl. Sci., 4 (2016).
[14] Y. Tan, M. Chen, Y. Hao, High efficient removal of Pb(II) by amino-functionalized $Fe_3O_4$ magnetic nano-particles, Chem. Eng. J., 191 (2012) 104–111.
[15] S.B. Khan, M. Ismail, E.M. Bakhsh, A.M. Asiri, Design of simple and efficient metal nanoparticles templated on ZnO-chitosan coated textile cotton towards the catalytic degradation of organic pollutants, J. Ind. Text., (2020) 1–26.
[16] S.S. Banerjee, D.-H. Chen, Fast removal of copper ions by gum arabic modified magnetic nano-adsorbent, J. Hazard. Mater., 147 (2007) 792–799.
[17] N. Neyaz, W.A. Siddiqui, K.K. Nair, Application of surface functionalized iron oxide nanomaterials as a nanosorbents in extraction of toxic heavy metals from ground water: a review, Int. J. Environ. Sci., 4 (2014) 472–483.
[18] Y.-J. Tang, L.-J. Wang, Z.-L. Xu, H.-Z. Zhang, Novel chitosan-piperazine composite nanofiltration membranes for the desalination of brackish water and seawater, J. Polym. Res., 25 (2018) 118.
[19] A.E. Karatapanis, D.E. Petrakis, C.D. Stalikas, A layered magnetic iron/iron oxide nanoscavenger for the analytical enrichment of ng-$L^{-1}$ concentration levels of heavy metals from water, Anal. Chim. Acta, 726 (2012) 22–27.
[20] A.S. Teja, P.-Y. Koh, Synthesis, properties, and applications of magnetic iron oxide nanoparticles, Prog. Cryst. Growth Charact. Mater., 55 (2009) 22–45.
[21] T. Fried, G. Shemer, G. Markovich, Ordered two-dimensional arrays of ferrite nanoparticles, Adv. Mater., 13 (2001) 1158–1161.
[22] Atul, M. Kumar, A. Sharma, I.K. Maurya, A. Thakur, S. Kumar, Synthesis of ultra small iron oxide and doped iron oxide nanostructures and their antimicrobial activities, J. Taibah Univ. Sci., 13 (2019) 280–285.
[23] Z.E. Gahrouei, S. Labbaf, A. Kermanpur, Cobalt doped magnetite nanoparticles: synthesis, characterization, optimization and suitability evaluations for magnetic hyperthermia applications, Physica E, 116 (2020) 113759.
[24] M.R. Awual, M.M. Hasan, J. Iqbal, M.A. Islam, A. Islam, S. Khandaker, A.M. Asiri, M.M. Rahman, Ligand based sustainable composite material for sensitive nickel(II) capturing in aqueous media, J. Environ. Chem. Eng., 8 (2020) 103591.
[25] S. Agarwal, N.B. Singh, Zinc ferrite–PVA nanocomposite and removal of chromium from aqueous solution, Emerging Mater. Res., 3 (2014) 222–229.
[26] M. Keshvardoostchokami, L. Babaei, A. Zamani, A. Parizanganeh, F. Piri, Synthesized chitosan/iron oxide nanocomposite and shrimp shell in removal of nickel, cadmium and lead from aqueous solution, Global J. Environ. Sci. Manage., 3 (2017) 267–278.
[27] M.F. Horst, M. Alvarez, V.L. Lassalle, Removal of heavy metals from wastewater using magnetic nanocomposites: analysis of the experimental conditions, Sep. Sci. Technol., 51 (2016) 550–563.
[28] X.W. Liu, Q. Hu, Z. Fang, X.J. Zhang, B.B. Zhang, Magnetic chitosan nanocomposites: a useful recyclable tool for heavy metal ion removal, Langmuir, 25 (2009) 3–8.
[29] R. Vijayakumar, Y. Koltypin, I. Felner, A. Gedanken, Sonochemical synthesis and characterization of pure nanometer-sized $Fe_3O_4$ particles, Mater. Sci. Eng. A, 286 (2000) 101–105.
[30] X.J. Wang, J.K. Song, J.Y. Huang, J. Zhang, X. Wang, R.R. Ma, J.Y. Wang, J.F. Zhao, Activated carbon-based magnetic $TiO_2$ photocatalyst codoped with iodine and nitrogen for organic pollution degradation, Appl. Surf. Sci., 390 (2016) 190–201.
[31] S. Gul, M. Ismail, M.I. Khan, S.B. Khan, A.M. Asiri, I.U. Rahman, M.A. Khan, M.A. Kamboh, Novel synthesis of silver nanoparticles using melon aqueous extract and evaluation of their feeding deterrent activity against housefly *Musca domestica*, Asian Pac. J. Trop. Dis., 6 (2016) 311–316.
[32] P. Mukherjee, A. Ahmad, D. Mandal, S. Senapati, S.R. Sainkar, M.I. Khan, R. Ramani, R. Parischa, P. Ajayakumar, M. Alam, Bioreduction of $AuCl_4^-$ ions by the fungus, *Verticillium* sp. and surface trapping of the gold nanoparticles formed, Angew. Chem. Int. Ed., 40 (2001) 3585–3588.
[33] D. Bhattacharya, R.K. Gupta, Nanotechnology and potential of microorganisms, Crit. Rev. Biotechnol., 25 (2005) 199–204.
[34] D. Anderson, J.L. Anthony, A. Chanda, G. Denison, M. Drolet, D. Fort, M. Joselevich, J.R. Whitfield, Green approaches: a new horizon for future scientists student voices from the Pan-American advanced studies institute on green chemistry, Green Chem., 6 (2004) G5–G9.
[35] M.N. Nadagouda, A.B. Castle, R.C. Murdock, S.M. Hussain, R.S. Varma, *In vitro* biocompatibility of nanoscale zerovalent iron particles (NZVI) synthesized using tea polyphenols, Green Chem., 12 (2010) 114–122.
[36] E.C. Njagi, H. Huang, L. Stafford, H. Genuino, H.M. Galindo, J.B. Collins, G.E. Hoag, S.L. Suib, Biosynthesis of iron and silver nanoparticles at room temperature using aqueous sorghum bran extracts, Langmuir, 27 (2011) 264–271.
[37] C.P. Kala, N.A. Farooquee, U. Dhar, Prioritization of medicinal plants on the basis of available knowledge, existing practices and use value status in Uttaranchal, India, Biodivers. Conserv., 13 (2004) 453–469.
[38] S. Adesina, The Nigerian *Zanthoxylum*; chemical and biological values, Afr. J. Trad. CAM, 2 (2005) 282–301.
[39] T. Koutzarova, S. Kolev, C. Ghelev, D. Paneva, I. Nedkov, Microstructural study and size control of iron oxide nanoparticles produced by microemulsion technique, Phys. Status Solidi C, 3 (2006) 1302–1307.
[40] A. Dolgormaa, C.-j. Lv, Y. Li, J. Yang, J.-x. Yang, P. Chen, H.-p. Wang, J. Huang, Adsorption of Cu(II) and Zn(II) ions from aqueous solution by gel/PVA-modified super-paramagnetic iron oxide nanoparticles, Molecules, 23 (2018) 2982.
[41] M. Ghaemy, S. Shabzendedar, M. Taghavi, One-step synthesis of poly(triazole-ether-quinoxaline) using click reaction: preparation and properties of magnetic nanocomposites with modified $Fe_3O_4$ for metal ions removal, J. Polym. Res., 21 (2014) 464.
[42] P. Loekitowati Hariani, M. Faizal, R. Ridwan, M. Marsi, D. Setiabudidaya, Synthesis and properties of $Fe_3O_4$ nanoparticles by co-precipitation method to removal procion dye, Int. J. Environ. Sci. Dev., 4 (2013) 336–340.
[43] I. Bibi, N. Nazar, S. Ata, M. Sultan, A. Ali, A. Abbas, K. Jilani, S. Kamal, F.M. Sarim, M.I. Khan, F. Jalal, M. Iqbal, Green synthesis of iron oxide nanoparticles using pomegranate seeds extract and photocatalytic activity evaluation for the degradation of textile dye, J. Mater. Res. Technol., 8 (2019) 6115–6124.
[44] E.J. Al-Kalifawi, Green synthesis of magnetite iron oxide nanoparticles by using Al-Abbas's (AS) hund fruit (*Citrus medica*) var. sarcodactylis swingle extract and used in Al-'alqami river water treatment, J. Nat. Sci. Res., 5 (2015) 125–135.
[45] M.E. Mahmoud, M.S. Abdelwahab, E.M. Fathallah, Design of novel nano-sorbents based on nano-magnetic iron oxide–bound-nano-silicon oxide–immobilized-triethylenetetramine for implementation in water treatment of heavy metals, Chem. Eng. J., 223 (2013) 318–327.
[46] M. Ismail, S. Gul, M. Khan, M.A. Khan, A.M. Asiri, S.B. Khan, Green synthesis of zerovalent copper nanoparticles for efficient reduction of toxic azo dyes Congo red and methyl orange, Green Process. Synth., 8 (2019) 135–143.
[47] M. Ismail, M. Khan, S.A. Khan, M. Qayum, M.A. Khan, Y. Anwar, K. Akhtar, A.M. Asiri, S.B. Khan, Green synthesis of antibacterial bimetallic Ag–Cu nanoparticles for catalytic reduction of persistent organic pollutants, J. Mater. Sci. – Mater. Electron., 29 (2018) 20840–20855.
[48] M. Ismail, M.I. Khan, K. Akhtar, J. Seo, M.A. Khan, A.M. Asiri, S.B. Khan, Phytosynthesis of silver nanoparticles; naked eye cellulose filter paper dual mechanism sensor for mercury ions and ammonia in aqueous solution, J. Mater. Sci. – Mater. Electron., 30 (2019) 7367–7383.

[49] M. Ismail, S. Gul, M.I. Khan, M.A. Khan, A.M. Asiri, S.B. Khan, Medicago polymorpha-mediated antibacterial silver nanoparticles in the reduction of methyl orange, Green Process. Synth., 8 (2019) 118–127.
[50] A. Bajpai, R. Gupta, Synthesis and characterization of magnetite ($Fe_3O_4$)—polyvinyl alcohol-based nanocomposites and study of superparamagnetism, Polym. Compos., 31 (2010) 245–255.
[51] M. Ismail, M.I. Khan, K. Akhtar, M.A. Khan, A.M. Asiri, S.B. Khan, Biosynthesis of silver nanoparticles: a colorimetric optical sensor for detection of hexavalent chromium and ammonia in aqueous solution, Physica E, 103 (2018) 367–376.
[52] U.A. Joshi, J.S. Lee, Template-free hydrothermal synthesis of single-crystalline barium titanate and strontium titanate nanowires, Small, 1 (2005) 1172–1176.
[53] Z. Es'haghi, F. Vafaeinezhad, S. Hooshmand, Green synthesis of magnetic iron nanoparticles coated by olive oil and verifying its efficiency in extraction of nickel from environmental samples via UV–vis spectrophotometry, Process Saf. Environ. Prot., 102 (2016) 403–409.
[54] E. Yan, M.L. Cao, J.Y. Jiang, J.W. Gao, C.C. Jiang, X.W. Ba, X.Y. Yang, D.-Q. Zhang, A novel adsorbent based on magnetic $Fe_3O_4$ contained polyvinyl alcohol/chitosan composite nanofibers for chromium(VI) removal, Solid State Sci., 72 (2017) 94–102.
[55] B. Gillot, R. Benloucif, X-ray diffraction, IR spectrometry and high resolution electron microscopy on ordered zinc-substituted maghemites, Mater. Chem. Phys., 32 (1992) 37–41.
[56] Y.-M. Hao, C. Man, Z.-B. Hu, Effective removal of Cu(II) ions from aqueous solution by amino-functionalized magnetic nanoparticles, J. Hazard. Mater., 184 (2010) 392–399.
[57] I. Langmuir, The constitution and fundamental properties of solids and liquids, Part I. Solids, J. Am. Chem. Soc., 38 (1916) 2221–2295.
[58] V.K. Gupta, A. Rastogi, A. Nayak, Biosorption of nickel onto treated alga (*Oedogonium hatei*): application of isotherm and kinetic models, J. Colloid Interface Sci., 342 (2010) 533–539.
[59] S. Nethaji, A. Sivasamy, A. Mandal, Adsorption isotherms, kinetics and mechanism for the adsorption of cationic and anionic dyes onto carbonaceous particles prepared from Juglans regia shell biomass, Int. J. Environ. Sci. Technol., 10 (2013) 231–242.
[60] Z.S. Pour, M. Ghaemy, Removal of dyes and heavy metal ions from water by magnetic hydrogel beads based on poly (vinyl alcohol)/carboxymethyl starch-g-poly(vinyl imidazole), RSC Adv., 5 (2015) 64106–64118.
[61] C. Cao, H.L. Kang, N. Che, Z.J. Liu, P.P. Li, C. Zhang, W.W. Li, R.G. Liu, Y. Huang, Wool graft polyacrylamidoxime as the adsorbent for both cationic and anionic toxic ions from aqueous solutions, RSC Adv., 4 (2014) 60609–60616.
[62] S. Debnath, K. Biswas, U.C. Ghosh, Removal of Ni(II) and Cr(VI) with titanium(IV) oxide nanoparticle agglomerates in fixed-bed columns, Ind. Eng. Chem. Res., 49 (2010) 2031–2039.
[63] S.-H. Huang, D.-H. Chen, Rapid removal of heavy metal cations and anions from aqueous solutions by an amino-functionalized magnetic nano-adsorbent, J. Hazard. Mater., 163 (2009) 174–179.